THE JOURNAL OF PHYSICAL CHEMISTRY B

Article

pubs.acs.org/JPCB

Processing of Surfactant Templated Nano-Structured Silica Films Using Compressed Carbon Dioxide as Interpreted from In Situ Fluorescence Spectroscopy

Kaustav Ghosh,[†,§] Stephen E. Rankin,[†] Hans-Joachim Lehmler,[‡] and Barbara L. Knutson*[,†]

[†]Department of Chemical and Materials Engineering, University of Kentucky, Lexington, Kentucky 40506-0046, United States

[‡]Department of Occupational and Environmental Health, University of Iowa, Iowa City, Iowa 52242-5000, United States

ABSTRACT: The local environment and dynamics of compressed carbon dioxide (CO_2) penetration in surfactant templated silica film synthesis is interpreted from the in situ fluorescence emission spectra of pyrene (Py) and a modified pyrene probe. Pyrene emission in cetyltrimethylammonium bromide (CTAB) and cetylpyridinium bromide (CPB) templated silica films is monitored immediately after casting and during processing with gaseous and supercritical (sc) CO_2 (17−172 bar, 45 °C). The solvatochromic emission spectra of pyrene in CTAB templated films suggest CO_2 penetration in both the micelle interface and its interior. An anchored derivative of pyrene, 1-pyrenehexadecanoic acid (C_{16}-pyr), is established for probing CPB films, where the pyrene moiety is preferentially oriented toward the micelle interior, thus limiting quenching by the pyridinium headgroup of CPB. CO_2 processing of CPB templated silica films results in an increase in the time scale for probe mobility, suggesting an increased time scale of silica condensation through CO_2 processing. The mobility of C_{16}-pyr increases with pressure from gaseous to sc CO_2 processing and persists for over 5 h for sc CO_2 processing at 172 bar and 45 °C compared to about 25 min for the unprocessed film. The delivery of CO_2 soluble solutes to specific regions of surfactant templated mesoporous materials is examined via the nonradiative energy transfer (NRET) between pyrene and CO_2-solubilized naphthalene.

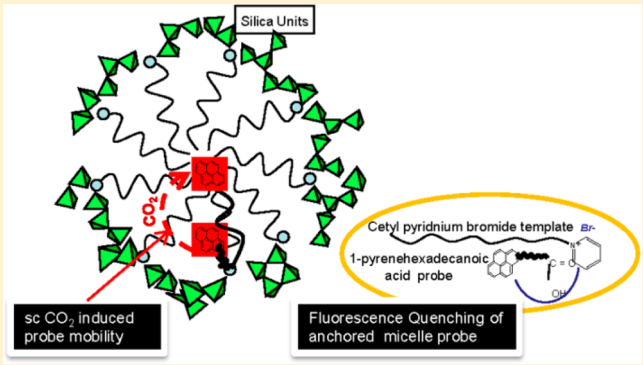

INTRODUCTION

The synthesis of mesoporous silica occurs through a coassembly process with the surfactant molecules forming ordered templates and the hydrolyzed silica precursor associating with the surfactant headgroup to form the solid silica network.[1] Subsequent silica condensation followed by removal of the surfactant results in ordered mesoporous silica with the mesostructure replicating the surfactant mesophase.[1] Tailoring the pore structure of surfactant templated materials has been demonstrated to increase the application of such materials.[2−4] Traditional methods of achieving pore expansion in surfactant templated silica have involved the addition of large hydrocarbon solvents (e.g., polypropylene oxide, dodecane, mesitylene, etc.) to the surfactant/silica precursor solution directly during the synthesis of porous silica to achieve pore expansion through swelling of the micelle core.[5−8]

Supercritical (sc) and compressed CO_2 processing has recently been used for the synthesis of tailored mesoporous silica through controlled CO_2 based swelling of the surfactant templates.[9−12] Sc CO_2 is an attractive alternative pore tailoring agent due to its tunable solvent strength, high diffusivity, and low surface tension, which enables diffusion through the nanometer sized pores while preserving the long-range structure. Pore expansion of up to 80% was achieved during the synthesis of templated silica thin films through CO_2 processing of "CO_2-philic" fluorinated templates (perfluoroalkyl pyridinium chloride surfactants with 8−10 fluorocarbon groups in the surfactant tail) at 172 bar and 45 °C.[11] In contrast, CO_2 pressures of 482 bar resulted in 54% pore expansion for a much longer hydrocarbon copolymer template (P123 with 69 propylene oxide (PPO) groups in its tail) through CO_2 uptake in the PPO core.[9] Negligible pore expansion was achieved for two other hydrocarbon surfactant templates, CTAB and CPB for processing pressures up to 172 bar.[9,13] Investigation of pore expansion between templates containing varying percentages of "CO_2-philic" fluorocarbon groups in their tails also suggested the ability of CO_2 to preferentially solvate "CO_2-philic" regions of the mesophase compared to "non-CO_2-philic" areas.[13]

Alteration of the pore structure of fluorinated surfactant templated dip-coated silica films by CO_2 occurs during the modulable steady state (MSS) of the synthesis.[11] During this period, which begins a few seconds after sol coating, silica condensation is in progress but is not sufficient to have formed a highly rigid network.[14] The application of external forces on

Received: May 25, 2012
Revised: August 31, 2012
Published: September 4, 2012

the flexible silica network during the MSS has been previously used to modify the final mesostructure of thin films.[14−17] The time scales of the MSS period also can be tuned through varying system parameters including relative humidity,[14] ethanol vapor pressure,[14] and surfactant template structure,[18] suggesting additional factors to engineer film mesostructure. Knowledge of localization of compressed CO_2 in the surfactant templated materials and the time scales of silica condensation during CO_2 processing can potentially be used to optimize mesoporous silica structure and functionalization during the MSS period.

The mechanism of penetration and localization of traditional hydrocarbon swelling agents in surfactant templated silica has been extensively investigated through experimental techniques such as small-angle X-ray scattering (SAXS)[5,8,19] and also described on the basis of the free energy of mixing.[20] As swelling agents, long chain alkanes (>C8) form an inner core, resulting in an increase in pore diameter, while shorter alkanes and aromatic hydrocarbons localize directly in the tail region with no change in micelle size.[8,19] In contrast, CO_2 processing of surfactant mesophases is not well studied, and experimental techniques have primarily employed small angle neutron scattering (SANS) to measure the swelling of surfactant mesophases as a function of CO_2 pressure and temperature.[21] The CO_2 penetration of dilute surfactant aggregates (i.e., CO_2-continuous microemulsions and emulsions) has been investigated more extensively[20,22,23] due to their potential application in enzymatic reactions,[23,24] extraction,[25] solublizing metal nanoparticles,[26,27] metal ions[28] and proteins,[29] and "green" applications of carbon dioxide technology.[30]

The in situ probing of the local environment of surfactant templated silica during CO_2 processing (i.e., through fluorescent spectroscopy probes) may provide additional insight into the localization and dynamics of CO_2 penetration in surfactant aggregates and mesostructures. Previously, fluorescence spectroscopy has been used to investigate the synthesis mechanism of surfactant templated mesoporous ceramics, the change in micelle polarity with the addition of additives during the synthesis, the mobility of various probes in sol−gel silica film and probe accessibility to the silica framework, the micelle core, and the micelle interface in a sol−gel silica film.[31−38] The solvatochromic behavior of pyrene, in particular, has been employed to follow in situ the interactions of surfactant and silica precursors in the synthesis of surfactant template mesoporous silica.[31,37] Pyrene[39] and other spectroscopic probe molecules[19,40,41] have also been incorporated in surfactant aggregates in both CO_2-continuous solutions and CO_2-swollen micelles to measure the polarity of their microenvironment.

In extending the use of high pressure fluorescence spectroscopy to measure the effects of CO_2 processing on the mesostructure of templated silica, the constrained thickness of silica thin films has a clear advantage over templated silica powders. At less than 500 nm in thickness, these films are expected to absorb very little intensity of the excitation beam. Previously, the diffusivity of pyrene in polymeric thin films of polystyrene due to compressed CO_2 processing was investigated through following the loss in pyrene fluorescence intensity with CO_2 processing time.[42] The diffusion coefficients and localization of fluorescence probes in CO_2 swollen polymer films have also been investigated in real time by high pressure fluorescence nonradiative energy transfer (NRET) using pyrene labeled polystyrene.[43]

This study examines the effect of CO_2 processing (17−172 bar, 45 °C) on hydrocarbon (CTAB and CPB) surfactant templated thin films using in situ high pressure fluorescence spectroscopy. The effect of CO_2 on the localization of pyrene, and pyrene derivatives, 1-pyrenedecanoic acid (C_{10}-pyr) and 1-pyrene hexadecanoic acid (C_{16}-pyr), in CTAB and CPB templated films is investigated. The time scales of silica condensation are inferred from the probe mobility in the thin film as a function of CO_2 processing condition and penetration times. CO_2 localization in surfactant templated silica is determined from the micropolarity of pyrene and the delivery and uptake of a solute dissolved in CO_2 to specific regions in surfactant templated films, as demonstrated using fluorescence nonradiative energy transfer (NRET) between pyrene and CO_2-solubilized naphthalene.

MATERIALS AND METHODS

Chemicals. The surfactants, cetyltrimethylammonium bromide (CTAB) and cetylpyridinium bromide (CPB), were obtained from Aldrich and used without further purification. Tetraethoxysilane (TEOS, purity >99%) was purchased from Gelest. Absolute ethyl alcohol purchased from Aaper Alcohol and Chemical Co. (Shelbyville, KY), deionized ultrafiltered water from Fisher Scientific, and hydrochloric acid (0.1 N standardized solution) obtained from Alfa Aesar were used for thin film synthesis. Carbon dioxide (Coleman grade, 99.99+%) and nitrogen (UltraHigh purity grade) were purchased from Scott Gross Co. (Lexington, KY). Decane (purity >99%) was obtained from Sigma Aldrich and used for thin film processing. The fluorescence probes, 1-pyrenedecanoic acid (C_{10}-pyr) and 1-pyrenehexadecanoic acid (C_{16}-pyr) (purity 99+%), were purchased from Molecular Probes. Pyrene was obtained from Sigma (purity ∼99%) and naphthalene (purity 98+%) from Fisher Scientific. Schematics of all surfactants and probes are presented in Figure 1.

Film Synthesis. The solution for silica film synthesis was prepared by first refluxing TEOS, ethanol, water, and HCl (mole ratio 1:3.8:1:5 × 10^{-5}) at 65 °C for 90 min to obtain a clear solution of partially hydrolyzed silica. The remainder of the required water and HCl were then added in calculated quantities, resulting in a nominal pH of approximately 2 in the final solution, and the mixture was aged at 25 °C for 15 min and then at 50 °C for an additional 15 min. Finally, a solution of the surfactant in ethanol was added to the previously hydrolyzed silica sol under constant stirring. The final mole ratios obtained were 1 TEOS:12 C_2H_5OH:5 H_2O:0.004 HCl:x surfactant (x = 0.06 for CTAB[44] and 0.1 for CPB[12]). The fluorescence probe (pyrene, C_{10}-pyr or C_{16}-pyr) was then added to the solution, resulting in a final probe concentration in the silica solution of 5 × 10^{-5} M. 500 μL of the silica solution was dropped on each side of a clean glass slide and allowed to spread to form a uniform film.

Atmospheric Fluorescence Measurements of Thin Films. Steady state fluorescence measurements of films without CO_2 processing were performed with a Varian Cary Eclipse fluorescence spectrophotometer (Walnut Creek, CA). The glass slides containing the surfactant templated silica films were mounted on the front face of a holder custom designed to fit in a cuvette holder and allow illumination by the excitation beam at an angle of 45°. A xenon pulse lamp was used as the light source, with an operational wavelength range of 200−900 nm (1.5 nm accuracy; {0.2 nm reproducibility}). Emission spectra of the pyrene or derivatized pyrene in the films were obtained

dx.doi.org/10.1021/jp305113b | J. Phys. Chem. B 2012, 116, 11646−11655

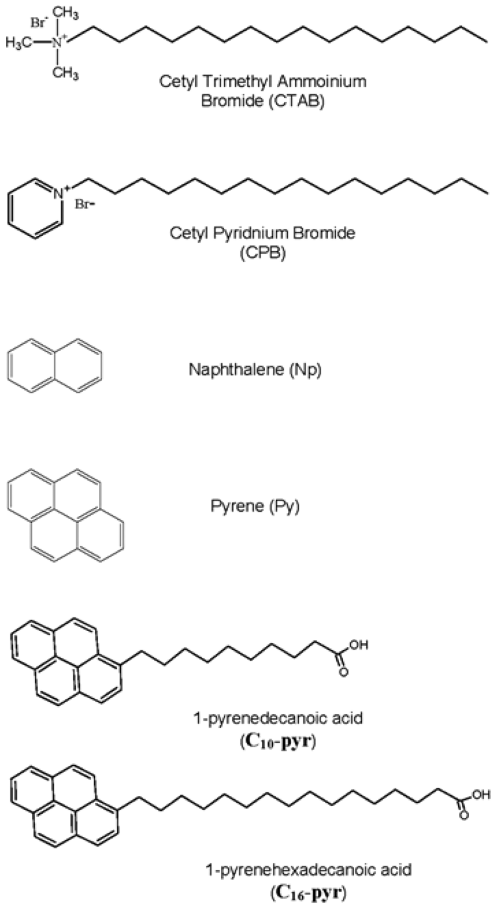

Figure 1. Schematic of CTAB, CPB, naphthalene, pyrene, and derivatives of pyrene.

by exciting the probe at 334 nm with an excitation slit width of 5 nm, an emission slit width of 1.5 nm, and the detector voltage set at 800 V.

High Pressure Fluorescence Spectroscopy of Thin Films. In situ fluorescence measurements of compressed CO_2 processing of silica film was conducted using a custom-designed film holder fitted inside a stainless steel variable volume view cell (10−25 mL working volume, rated to 20.7 MPa) obtained from Thar Technologies (Pittsburgh, PA). The high pressure cell was mounted within the sample compartment of the Varian Cary Eclipse fluorescence spectrophotometer (Figure 2). The film holder was placed in line with the quartz windows such that the beam illuminates the film at 45°. The film was kept in a

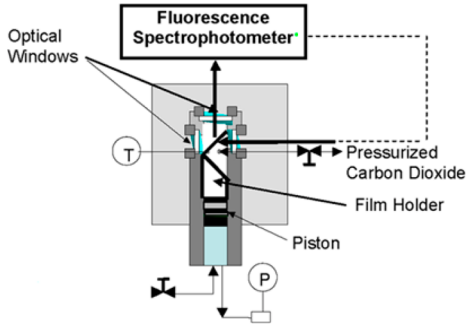

Figure 2. Apparatus for high pressure thin film fluorescence measurements.

constant position during CO_2 pressurization by using a constant volume of an overburden incompressible fluid (water) on the other side of a floating O-ring piston away from the film holder (Figure 2), which restricted movement of the film holder throughout CO_2 injection. The temperature of the spectroscopic cell was controlled using an Omega controller (model CN9000A) with heating tape.

After coating, the films were mounted in the high pressure view cell and the fluorescence of the probe molecules in the films was monitored for two film aging times, which is defined as the time period between depositing the solution and initiating the CO_2 processing of the film. Film aging times of less than 5 min (briefly aged films) and greater than 25 min (well-aged films) were investigated. After aging, the pressure of CO_2 in the cell was increased at a rate of 15 bar/min until the desired pressure was reached (17−172 bar). CO_2 was deoxygenated by passing it through a high pressure oxygen trap (Alltech, rated to 125 bar) and supplied to the view cell using an Isco syringe pump (Lincoln, NE, model 500D). Deoxygenated CO_2 was used to prevent collisional quenching of the probe by molecular oxygen. Films were maintained at the desired CO_2 pressure at 45 °C for up to 24 h, as described in the individual experiments. This procedure for CO_2 pressurization has been previously demonstrated to preserve the long-range pore structure of surfactant templated silica films.[11] Emission spectra of pyrene in CTAB templated film and C_{16}-pyr in CPB templated film were obtained at specific intervals during CO_2 processing by exciting the probes at 334 nm.

Nonradiative energy transfer (NRET) was measured between naphthalene (donor) and C_{16}-pyr (acceptor). Naphthalene was dissolved in deoxygenated CO_2 at a fixed concentration of 5×10^{-5} M and supplied to the view cell using an Isco syringe pump. C_{16}-pyr labeled CTAB templated films were produced as described above. With naphthalene present in the system, the sample was excited at 290 nm and fluorescence spectra were recorded in the wavelength range 300−550 nm. The ratio of the intensities of C_{16}-pyr fluorescence to naphthalene fluorescence (I_P/I_N) is a measure for NRET efficiency[45,46] and was calculated from fluorescence intensities at 338 and 376 nm for naphthalene and C_{16}-pyr emission, respectively.

RESULTS AND DISCUSSION

Fluorescence Spectroscopy of Silica Films without CO_2 Processing. The application of the fluorescence probe systems (pyrene, C_{10}-pyr, C_{16}-pyr) is first demonstrated for probing non-CO_2 processed silica thin films templated with the hydrocarbon surfactants CTAB and CPB, prior to investigating the localization of CO_2 and delivery of CO_2 solubilized solute to the surfactant templated materials. The solvatochromic probe pyrene has been extensively used to investigate systems both at low pressure[47−50] and in compressed CO_2 environments.[51,52] The micropolarity of pyrene's local environment is inferred from the ratio of the fluorescence intensities of the vibronic bands of pyrene (intensity ratio of first to third band, I1/I3). The value of the I1/I3 ratio varies from 0.6 for a nonpolar solvent, such as hexane, to 1.8 for an aqueous environment.[47]

Figure 3 presents schematically the surfactant templating mechanism to synthesize ordered mesoporous silica film through dip-coating and localization of the surfactant and silica matrix in the silica thin film during the aging process. The emission spectrum of pyrene in a CTAB templated film without

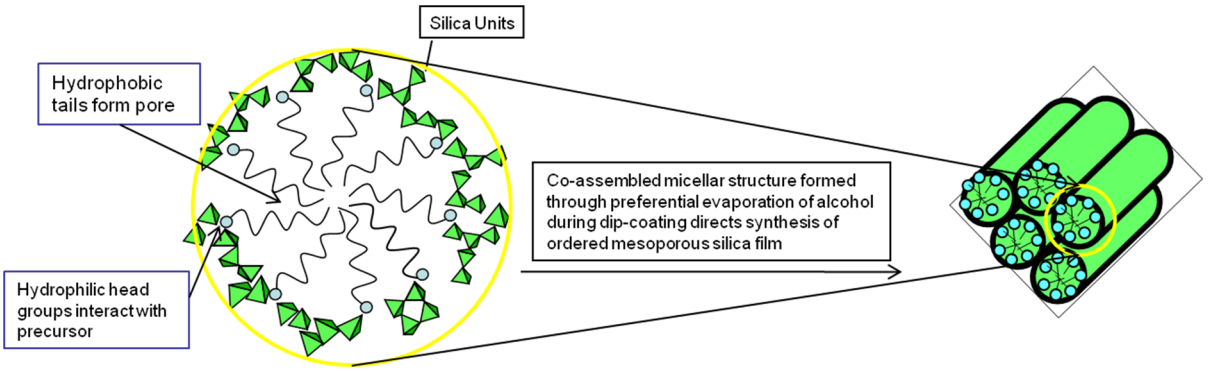

Figure 3. Schematic of synthesis of surfactant templated ordered mesoporous silica thin film through dip-coating.

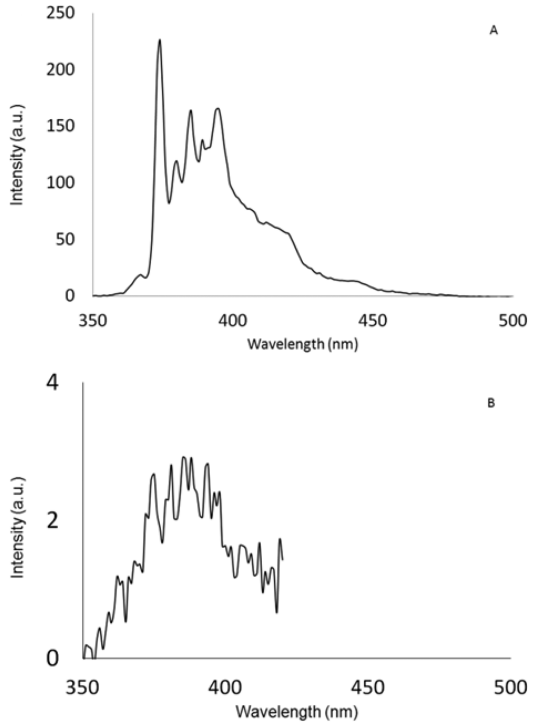

Figure 4. Emission spectra of pyrene in (A) CTAB and (B) CPB templated film without CO_2 processing.

CO_2 processing is presented in Figure 4a. The spectrum displays five sharp vibronic bands, characteristic of pyrene fluorescence at low probe concentration, with an I1/I3 value of 1.4. The value of I1/I3, which is intermediate between that for a polar and a nonpolar solvent environment, suggests the presence of pyrene at the interface of the CTAB micelle, consistent with previous studies.[47,48] Alternatively, excitation of pyrene in a CPB templated film results in negligible emission intensity (Figure 4b). Similar to CTAB micelles, pyrene is also expected to be present at the CPB micelle interface. However, pyrene fluorescence is effectively quenched by the pyridinium headgroup of CPB at the interface through electron transfer from the photoexcited state of pyrene to the electron deficient pyridinium group, leading to the decreased emission intensity.[53,54] In CPB micelles, quenching of pyrene probes occurs through static quenching, in which the electron transfer from the excited probe to the nearest pyridinium neighbor requires no pyrene diffusion because of the high local concentration of the quencher.[55,56]

The modification of pyrene with a carboxylic acid tail is expected to significantly alter the location of the pyrene moiety in a CTAB or CPB micelle. The conformation of pyrene fatty acids in self-assembled aggregates is a function of the fatty-acid chain length, interaction of the carboxylic moiety with surface active agent headgroup, and the shape and rigidity of the self-assembled structure.[57−61] Investigations of self-assembled lamellar structures including Langmuir−Blodgett monolayers and unilamellar vesicles suggest that the carboxylic acid group associates at the aggregate interface with the pyrene chromophore localized with deeper penetration in the micelle core with increasing fatty-acid chain length.[57−59] Similar to lamellar aggregates, derivatized pyrene localization in more open cylindrical micelles is in the micelle interior with the carboxylic group associated at the micelle interface.[60,61] However, the exact conformation of fatty acid pyrene derivatives in cylindrical micelles is specific to the probe−micelle system. In sodium doceylsulfate (SDS) micelles, increasing pyrene penetration in the micelle interior was demonstrated with increasing fatty acid chain length from C_3 to C_{15}.[60] In contrast, the pyrene moieties of 1-pyrenebutanoic acid (C_4-pyr), 1-pyrenenonanoic acid (C_9-pyr), 1-pyrenedodecanoic acid (C_{12}-pyr), and C_{16}-pyr were all located at the same depth in the cetyltrimethylammonium chloride (CTAC) micelle interior.[61] Anchoring of fatty acid pyrene derivative at the micelle interface and orientation of the pyrene chromophore in the micelle interior in the current study would be a potential advantage of probing CPB templated films, as it limits the quenching of pyrene by the pyridine headgroup.

The location of derivatized pyrenes C_{10}-pyr and C_{16}-pyr in non-CO_2 processed silica films templated by CTAB and CPB (Figure 5) is inferred from their emission spectra. For CTAB templated films, both derivatized probes display emission spectra with high intensity (Figure 5a and b). In contrast, in CPB templated films, the intensity of the emission spectra of C_{10}-pyr is negligible (Figure 5c), while significant emission intensity is observed for the longer hydrocarbon chain probe, C_{16}-pyr, in CPB templated film (Figure 5d). The low intensity of C_{10}-pyr suggests quenching of the pyrene moiety, possibly by a static quenching mechanism similar to the free quenching of pyrene observed previously in CPB micelles,[55] indicating C_{10}-pyr chromophore localization close to the micelle interface.

The significant fluorescent intensity of the longer chain C_{16}-pyr in CPB templated material (Figure 5d) is consistent with the pyrene moiety being located in the interior of the micelle. Thus, the penetration of the pyrene chromophore in the micelle interior for the longer chain C_{16}-pyr is greater compared to C_{10}-pyr. C_{16}-pyr has the same number of hydrocarbon

dx.doi.org/10.1021/jp305113b | J. Phys. Chem. B 2012, 116, 11646−11655

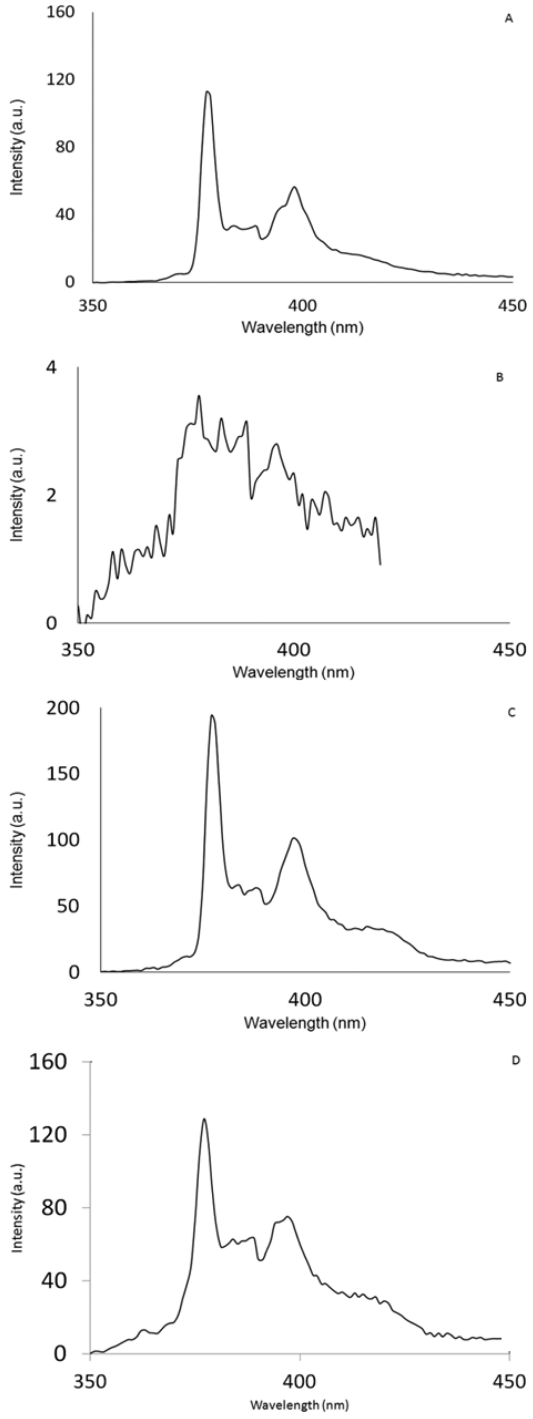

Figure 5. Emission spectra of C_{10}-pyr in (A) CTAB and (B) CPB and C_{16}-pyr in (C) CTAB and (D) CPB templated film.

groups as CPB (16 carbons), and favorable interactions between hydrocarbon chains of identical lengths may result in localization of the pyrene moiety of C_{16}-pyr in the micelle interior of CPB templated films, as observed previously for functional group incorporation in the micelles of surfactant templated materials.[62] While localization and high fluorescent intensities in the CPB templated films are an advantage of the C_{16}-pyr probe, a disadvantage is the loss of its solvatochromic emission upon functionalization of pyrene. The solvent dependence emission of pyrene is a result of solute−solvent dipole−dipole coupling and π-orbital coupling and is dependent on the symmetry of pyrene,[47] which is lost for C_{16}-pyr. However, the location of the pyrene moiety in the micelle interior for the anchored C_{16}-pyr is advantageous for probing CO_2 interactions and CO_2 based solute delivery in the micelle interior, as described below.

CO_2 Solvation and Time Scales of Silica Condensation with CO_2 Processing. The period of continuous silica condensation in the synthesis of dip-coated surfactant templated thin film is referred to as the modulable steady state (MSS).[14] Previously, researchers have modified thin film structure during the MSS by changing system humidity,[14] ethanol vapor concentration,[15] and surface chemistry of the substrate[17] and by applying an external magnetic field to alter the thin film orientation.[16] Extending the MSS period may increase opportunities to tailor the mesostructure of thin films by directly altering the pore size, structure, or functional group incorporation.

Our previous study suggests that the alteration of pore structure through compressed CO_2 processing of fluorinated surfactant templated silica film also occurs during the MSS period.[11] Specifically, the resulting XRD patterns of fluorinated surfactant templated thin films changed progressively during the first 12 h of CO_2 processing, suggesting continuous changes in mesoporous silica structure during that time period. This change in mesostructure can be attributed to ongoing silica condensation and a prolonged MSS phase during CO_2 processing, which would represent a significant extension in condensation time scales relative to unprocessed films. For example, IR spectra measurements of silanol bond intensity as a function of aging time for a CTAB templated acid catalyzed silica film aged in ambient conditions showed a constant value after about 20 min of aging time, suggesting significant progress of silica condensation and MSS phase for the CTAB templated film.[18] Silica condensation time scales in acid catalyzed films have been demonstrated to be tunable through varying relative humidity with a less humid environment, promoting quicker water evaporation from the film and decreasing condensation time scales.[14] The MSS time period during the synthesis of acid catalyzed surfactant templated silica film is also dependent on the template structure with a larger template headgroup leading to increased time scales of silica condensation.[18] Even though CTAB and CPB templated materials do not demonstrate significant CO_2 based pore expansion,[9,12] the possibility of extending condensation time scales for further pore engineering of such materials exists if CO_2 penetration occurs in those templates.

CO_2 localization during processing of CTAB templated silica film is interpreted from the time dependent in situ fluorescence spectra of the pyrene probes in acid-catalyzed CTAB templated films for both the briefly aged films (aging time <5 min prior to exposure to CO_2) and the well-aged films (aging time >25 min). The extent of silica condensation is expected to be significant for the well-aged films before being processed in CO_2 compared to a much decreased condensation for the briefly aged films.[18] Figure 6a plots the ratio of the intensity of the third vibronic emission band of pyrene (I3, emission at 385 nm) with increasing CO_2 processing time (at 45 °C and 103 bar) to its initial intensity ($I3_0$) for CTAB templated films of both aging times. I3 is insensitive to solvent polarity, and hence, a decrease in the value of I3 indicates an overall decrease in pyrene emission intensity. Significant and similar intensity decreases, to 30% of the initial values, are observed for films of both aging times through the first 6 h of CO_2 processing. Since

dx.doi.org/10.1021/jp305113b | J. Phys. Chem. B 2012, 116, 11646−11655

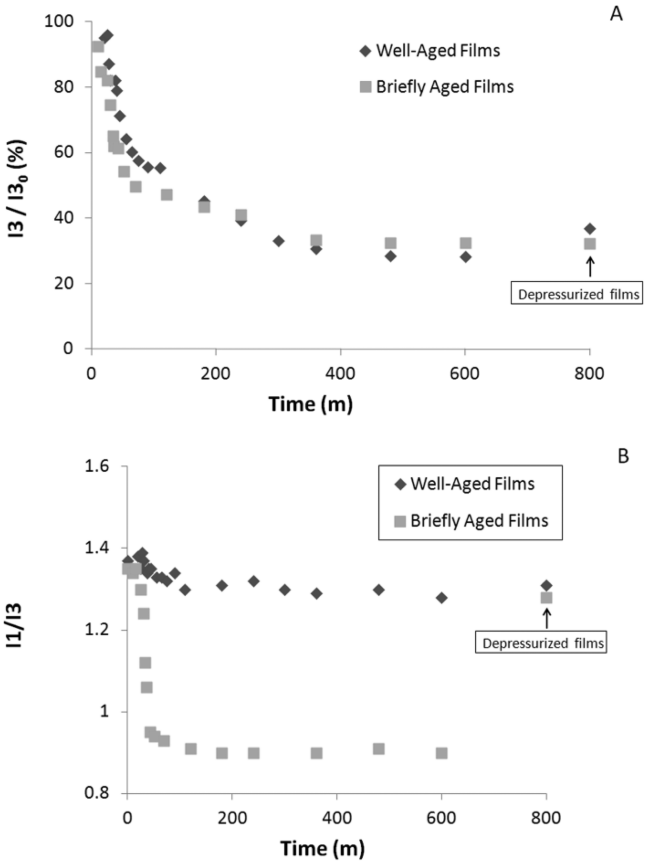

Figure 6. (A) Change in emission intensity and (B) I1/I3 values of pyrene spectra in CTAB templated film and processed in CO_2 at 103 bar and 45 °C.

pyrene quenching is not significant in CTAB micelles,[47,48] the decrease in the emission intensity of pyrene is due to the leaching of pyrene from the film into the bulk CO_2. The emission intensity from pyrene in bulk CO_2 is negligible compared to pyrene emission from the thin film due to pyrene's reduced concentration in bulk CO_2, and a decrease in the total emission intensity is expected with leaching. The dissolution of pyrene from polymeric films into bulk compressed CO_2 has been previously reported.[43]

Further, depressurization of the system after 12 h does not result in an appreciable increase in pyrene intensity. This suggests that pyrene remains dissolved in CO_2 during depressurization and does not redeposit in the film. To further confirm the dissolution of pyrene in CO_2, the pyrene dissolved in CO_2 was captured by bubbling in ethanol during depressurization. Significant quantities of pyrene were solubilized in the depressurized CO_2, as measured by fluorescence spectroscopy of the ethanol solution (spectra not shown). The similar rate and extent of pyrene leaching for films of both aging times suggests that accessibility of pyrene in the CTAB templated film and its subsequent solubilization in sc CO_2 is not significantly dependent on the extent of silica condensation.

The solvatochromic behavior of pyrene provides further insight into the localization of CO_2 in the surfactant templated films. Figure 6b presents the I1/I3 ratios for pyrene emission in CTAB film for CO_2 processing at 103 bar and 45 °C as a function of processing time for films of both aging times. The I1/I3 ratio for the briefly aged films decreases from 1.4 (for a nonprocessed film) to about 0.9 within the first 20 min of CO_2 processing and remains constant thereafter. The decrease in I1/I3 value indicates a change in localization of pyrene remaining in the briefly aged films from a micellar interface to a considerably less polar environment, consistent with CO_2 solubilization of pyrene and localization in the nonpolar micelle interior. Indeed, pyrene present at micelle interfaces has been demonstrated to be solubilized by compressed CO_2 into the micelle interior.[19,60] Interestingly, CO_2 penetration in the micelle interior occurs even for this hydrocarbon surfactant template, which shows no significant pore expansion when processed with CO_2.[9] Similar solvent penetration in surfactant tails without micelle expansion has been observed for alcohols and aromatic hydrocarbons.[8]

In contrast to the briefly aged films, no significant change in the I1/I3 ratio of pyrene was observed for the well-aged film with CO_2 processing, suggesting that pyrene remaining in the well-aged film throughout CO_2 processing is localized at the film interface and does not diffuse into the micelle interior. The decreased diffusivity of pyrene is attributed to the significantly condensed nature of the silica matrix resulting from the longer film aging period before CO_2 processing. The dependence of pyrene diffusivity on the rigidity of film structure has been noted previously through observation of decreasing diffusion rate of pyrene in PDMS resins with increasing cross-linking of the polymer chains.[63] For films of both aging times, the I1/I3 ratio is approximately 1.35 after CO_2 depressurization, indicating that the environmental change in the vicinity of pyrene is reversible in the briefly aged film. During CO_2 depressurization, pyrene localization in the briefly aged film changes from the micelle interior back to the interface.

The preferential location of the pyrene group of C_{16}-pyr in the micelle interior for CPB templated silica films is used to investigate the localization of CO_2 and the time frame of silica condensation in the films as a function of CO_2 processing time and conditions. Anchoring of the probe system to the micelle interface also results in insignificant CO_2-based leaching of C_{16}-pyr from the cationic surfactant templated films, as determined from the negligible change in C_{16}-pyr emission intensity in briefly aged CTAB templated film for CO_2 processing at 103 bar and 45 °C (not shown).

The emission intensity of C_{16}-pyr is reported for the first and most prominent vibronic emission band (I1) of this non-solvatochromic probe. Figure 7 plots the change in emission intensity of C_{16}-pyr in CPB templated film ($I1/I1_0$ where $I1_0$ is the value of I1 before initiating CO_2 processing) as a function

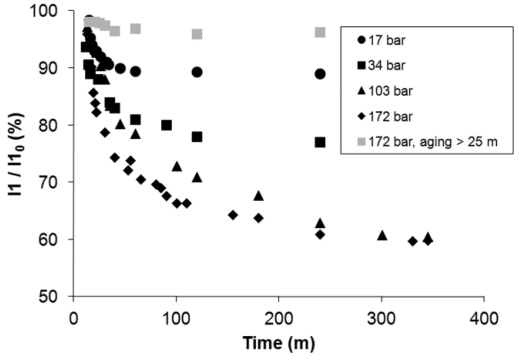

Figure 7. Change in emission intensity of C_{16}-pyr in CPB templated film and processed in CO_2 at different pressures and 45 °C as a function of processing time.

dx.doi.org/10.1021/jp305113b | J. Phys. Chem. B 2012, 116, 11646–11655

of CO_2 processing time and conditions for both film aging times. Significant decreases in C_{16}-pyr emission intensity at processing times greater than 1 h are observed for the briefly aged films at all conditions of CO_2 processing compared to the nonprocessed films. In the absence of probe leaching, the decrease in emission intensity of C_{16}-pyr is attributed to the quenching of the pyrene moiety by the pyridinium headgroup of the surfactant. The quenching is consistent with continued C_{16}-pyr mobility in the micelle interior, leading to increased interactions of the probe with pyridine. Enhanced probe mobility in the micelle interior is hypothesized to occur in the briefly aged films due to the reduced extent of silica condensation, providing a more flexible silica network during CO_2 processing. In contrast, the emission intensity of C_{16}-pyr in the well-aged CPB films remains essentially constant with time for CO_2 processing at 103 bar and 45 °C, suggesting that probe mobility even with CO_2 processing is negligible in films having significant silica condensation. Indeed, it has been previously demonstrated that the diffusion of redox active probes in silica sol−gel glass decreases significantly with increasing silica condensation during the initial gelation period.[64]

The mobility of C_{16}-pyr in the briefly aged films is a function of CO_2 processing conditions. In gaseous CO_2 processing, increasing pressure results in greater reductions of the emission intensity of the chromophore (17 bar and 45 °C, 90% of original intensity; 34 bar and 45 °C, ∼80% of original intensity). Processing the silica films in sc CO_2 at 103 bar and 45 °C results in a final intensity of ∼60% the original value, but the emission does not decrease further with increasing pressure. The time frame for probe mobility, as measured by its decrease in the emission intensity of C_{16}-pyr, also varies with CO_2 conditions. The emission intensity of C_{16}-pyr in gaseous CO_2 processed films reaches a constant value after approximately 2 h, whereas C_{16}-pyr intensity continues to decrease for the films processed in sc CO_2 for at least 5 h.

C_{16}-pyr mobility in films processed in CO_2 is hypothesized to decrease with processing time for all CO_2 conditions (Figure 7) due to progressive silica condensation, which would limit the association of pyrene moiety with pyridine group. A time frame of 5 h of continuous probe mobility during sc CO_2 processing of acid catalyzed CPB templated film represents an increase in the silica condensation time scales compared to non-CO_2 processed films.[18]

Several possible hypotheses explain potential mechanisms through which compressed CO_2 processing of acid catalyzed surfactant templated silica film can decrease the progress of silica condensation. The silica condensation rate is minimized under acidic conditions, at a pH between 2 and 4. Compressed CO_2, which acidifies aqueous solutions (pH ∼ 3) through formation and dissociation of carbonic acid,[40] is expected to decrease silica condensation to a greater extent than ambient air. In addition, acid catalyzed silica condensation proceeds through a series of condensation reactions with a key participant being an electrophilic moiety, a protonated silanol intermediate ($SiOH_2^+$).[66] The use of compressed CO_2 as a processing solvent during silica condensation is expected to stabilize this electrophilic intermediate through electrostatic interactions with the electronegative oxygen atoms in CO_2 or HCO_3^-, weakening the driving force for it to act as a leaving group and resulting in a decrease in the rate of the subsequent condensation reaction. Further increase of CO_2 concentration in the silica film with processing pressure (at a constant temperature for the same volume of film) is expected to increase the stabilization of $SiOH_2^+$ molecules, resulting in an increase in silica condensation time scales. This leads to extended mobility of a greater number of C16-pyr probes in the silica matrix with increasing CO_2 pressure, which is consistent with the observed increase in fluorescence quenching for C16-pyr for sc CO_2 compared to gaseous CO_2 processing (∼60% I1/Io (%) for sc CO_2 processing at 172 bar, 45 °C vs 80% I1/Io (%) for gaseous CO_2 at 34 bar, 45 °C − Figure 7). Similar decreases in silica condensation rate through electrostatic interaction between processing solvents and reaction intermediates to stabilize the intermediates have been demonstrated previously for both acid and base catalyzed condensation reactions.[65,67,68]

The silica condensation rate in acid catalyzed surfactant templated films also decreases with a decrease in the rate of water evaporation from the film.[69] The solubility of water in compressed CO_2 at 172 bar and 45 °C is about 0.007 mol of H_2O/mol of CO_2 or 0.003 g of H_2O/g of CO_2.[70] In contrast, the solubility of water in air at 45 °C and at ambient pressure is 0.058 g of H_2O/g of air.[71] Thus, the driving force for water evaporation is greater at ambient conditions than in a CO_2 environment, potentially reducing its rate of evaporation and the rate of silica condensation. The solubility of water in CO_2 gradually increases with CO_2 pressure.[70] In addition, the extraction of water from silica surfaces increases significantly in sc CO_2 compared to the gaseous CO_2 environment.[72] The combination of these trends suggests greater removal of water from silica film at sc CO_2 compared to gaseous CO_2 conditions, indicating increased progress in silica condensation at sc CO_2 condition. Thus, while the effect of water evaporation from the film is consistent with an observed decrease in silica condensation kinetics for aging in compressed CO_2 versus ambient conditions, it does not explain the observed pressure effect (slower aging in gaseous CO_2 versus supercritical CO_2). Changes to the residual water in the film with solvent environment may not be the predominant mechanism that affects silica condensation in this system.

High Pressure Nonradiative Energy Transfer. The preferential localization of the pyrene moiety in the micelle interior for the anchored probe, C_{16}-pyr, suggests the opportunity to investigate the delivery of CO_2 dissolved solutes to the micelle interior. NRET involving anchored probes has previously been used to investigate solvent and water uptake in micelle and microemulsion systems.[73,74] Naphthalene and pyrene are often used as an energy donor/acceptor pair;[45,46,75,76] naphthalene emission and pyrene absorption have a large spectral overlap, and the excitation of the system at 290 nm is selective to naphthalene.[46]

In this study, CO_2 with solubilized naphthalene is directly used for processing of the briefly aged CTAB templated film. As supported by our experiments, C_{16}-pyr is anchored to the micelle interface through its carboxylic acid tail and the pyrene moiety present in the micelle interior is used as the electron acceptor. Energy transfer between naphthalene and C_{16}-pyr would suggest a high probability of naphthalene colocalization in the same micelle interior domain with the pyrene group.[77] The high solubility of naphthalene in compressed CO_2 is well documented[78,79] and is an additional advantage of this probe system. A naphthalene concentration in CO_2 of 5×10^{-5} M can be achieved over the CO_2 temperatures and pressures of this investigation.[80,81]

NRET between naphthalene and C_{16}-pyr is confirmed from the emission spectra of a briefly aged CTAB templated film (labeled with C_{16}-pyr) processed with naphthalene solubilized CO_2 at 103 bar and 45 °C (Figure 8). In the absence of

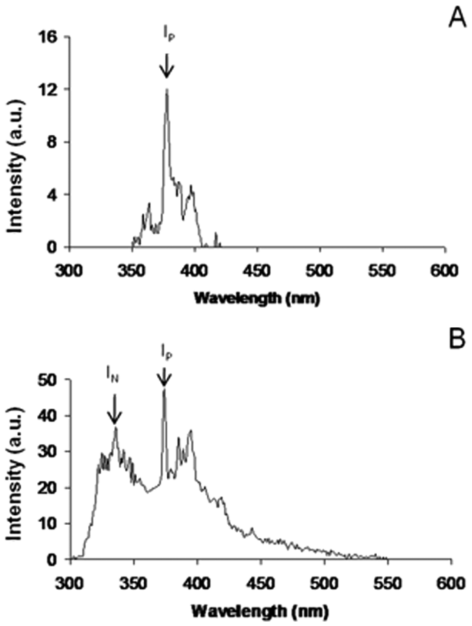

Figure 8. Emission spectra of C_{16}-pyr in CTAB templated film excited at 290 nm and processed in CO_2 at 103 bar and 45 °C (A) without dissolved naphthalene and (B) with naphthalene.

naphthalene, excitation of the C_{16}-pyr labeled CTAB templated film at 290 nm displays a weak emission around 377 nm (Figure 8a). However, with the introduction of naphthalene dissolved in CO_2, the emission intensity of C_{16}-pyr around 377 nm is significantly increased, along with a corresponding emission from naphthalene around 340 nm (Figure 8b). These emission spectra characteristics demonstrate energy transfer between naphthalene and the pyrene moiety of C_{16}-pyr and suggest naphthalene localization in the micelle interior, as also demonstrated in naphthalene−CO_2−Pluronic block copolymer micellar systems.[82] In the absence of CO_2, naphthalene is expected to reside at micelle interfaces.[56] Naphthalene localization in the micelle interior for CTAB templated film during CO_2 processing, as observed from NRET, thus indicates CO_2 solubilization of naphthalene for delivery of naphthalene into the micelle interior.

The efficiency of energy transfer between naphthalene and C_{16}-pyr can be used to interpret the naphthalene uptake in the CTAB templated films. Efficiency of energy transfer is calculated using the ratio of the fluorescence intensities of the acceptor to the donor (I_P/I_N, where I_P is pyrene emission at 377 nm and I_N is naphthalene emission at 338 nm) and is plotted in Figure 9 as a function of processing pressure and time. The I_P/I_N ratio increases rapidly and has similar values at all CO_2 processing conditions for the first 1 h of processing ($I_P/I_N \sim 0.95$ at 1 h), suggesting similar naphthalene delivery in the briefly aged CTAB template film for all CO_2 conditions during the first hour of CO_2 processing. Thereafter, the I_P/I_N ratio is approximately constant for gaseous CO_2 processing but continues to increase for sc CO_2 processing. The final I_P/I_N ratios increase with processing pressure from gaseous (from 34 bar ($I_P/I_N \sim 0.96$) to 69 bar ($I_P/I_N \sim 1.02$) at 45 °C) to sc CO_2

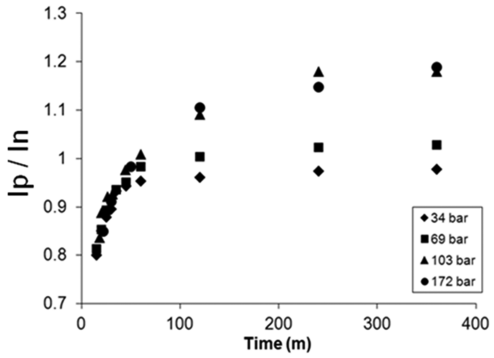

Figure 9. I_P/I_N ratios due to NRET between naphthalene solubilized in processing CO_2 and C_{16}-pyr in CTAB templated film as a function of processing time and pressure.

conditions (172 bar at 45 °C, $I_P/I_N \sim 1.2$) consistent with greater naphthalene uptake for sc CO_2 processing compared to gaseous CO_2 processing. Different conditions of sc CO_2 processing (103 and 172 bar at 45 °C) lead to a similar final ratio of I_P/I_N (~1.2). The efficiency of energy transfer was constant after about 1.5 h for gaseous CO_2 processing but continued to increase for at least 4 h of processing times for sc CO_2. These results establish the extended time scales for compressed CO_2 based transport of the soluble solute, naphthalene in the micelle interior for briefly aged acid catalyzed silica films as a function of CO_2 processing pressures.

CONCLUSIONS

Fluorescence spectroscopy was established as a novel technique to investigate the penetration of compressed CO_2 in surfactant templated silica films. 1-Pyrenehexadecanoic acid was established as a probe system to estimate in situ the localization of compressed CO_2, silica condensation time scales, and CO_2 solubilized solute delivery in the templated silica films. The potential of CO_2 processing to alter templated thin film structures through penetration in the surfactant tail and extension of silica condensation time scales was demonstrated for hydrocarbon surfactant (CTAB and CPB) templated silica, for which negligible pore expansion has been observed previously. CO_2 processing of CPB templated films increases the time frame of mobility, from about 20 min for non-CO_2 processed films to about 5 h during sc CO_2 processing. The transport of a soluble solute in CO_2, naphthalene, to the micelle interior of CTAB templated silica film was demonstrated for up to 4 h of sc CO_2 processing.

The ability to transport solubilized small solutes in mesoporous silica using CO_2 suggests its application in delivery of drug molecules, reactants, and novel functional groups. Sc CO_2 is able to access silanol groups in mesoporous silica that are "inaccessible" to traditional liquid solvents due to its favorable transport properties.[83] Sc CO_2 has also been used to load and encapsulate drugs into polymers and nanoparticles,[84−86] while mesoporous silica with tailored pore sizes has been used for adsorption of drugs for subsequent controlled release.[2] The potential exists for application of sc CO_2 to load drug molecules and functional groups in mesoporous silica while simultaneously extending silica condensation, thus suggesting a more uniform distribution of solutes and loading in more "inaccessible" regions than possible for CO_2 processing after complete silica condensation. Knowledge of the time scales of silica condensation and the localization of solute/

dx.doi.org/10.1021/jp305113b | J. Phys. Chem. B 2012, 116, 11646−11655

reactant molecules as a function of CO_2 processing time and pressure allows for the optimization of the solute loading and release in mesoporous materials.

AUTHOR INFORMATION

Corresponding Author

*Phone: 859-257-5715. Fax: 859-323-1929. E-mail: bknutson@engr.uky.edu.

Present Address

[§]Whirlpool Corporation, Research & Engineering, 750 Monte Road, Benton Harbor, MI 49022.

Notes

The authors declare no competing financial interest.

ACKNOWLEDGMENTS

The authors would like to acknowledge National Science Foundation NIRT Grant # DMR-0210517 and Kentucky Science and Engineering Foundation grant KSEF-159-RDE-001 for funding of this research project.

REFERENCES

(1) Beck, J. S. V., J. C.; Roth, W. J.; Leonowicz, M. E.; Kresge, C. T.; Schmitt, K. T.; Chu, C. T.-W.; Olson, D. H.; Sheppard, E. W.; McCullen, S. B.; Higgins, J. B.; Schlenker, J. L. *J. Am. Chem. Soc.* **1992**, *114*, 10834.

(2) Qu, F.; Zhu, G.; Lin, H.; Zhang, W.; Sun, J.; Li, S.; Qiu, S. *J. Solid State Chem.* **2006**, *179*, 2027.

(3) Ma, Y.; Qi, L.; Ma, J.; Wu, Y.; Liu, O.; Cheng, H. *Colloids Surf., A* **2003**, *229*, 1.

(4) Fuertes, A. B.; Lota, G.; Centeno, T. A.; Frackowiak, E. *Electrochim. Acta* **2005**, *50*, 2799.

(5) Blin, J. L.; Otjacques, C.; Herrier, G.; Su, B. *Langmuir* **2000**, *16*, 4229.

(6) Branton, P. J.; Doughert, J.; Lockhart, G.; White, J. W. *Charact. Porous Solids IV* **1997**, 668.

(7) Kimura, T.; Sugahara, Y.; Kuroda, K. *Chem. Commun.* **1998**, 559.

(8) Kunieda, H.; Ozawa, K.; Huang, K. L. *J. Phys. Chem. B* **1998**, *102*, 831.

(9) Hanrahan, J. P.; Copley, M. P.; Ziegler, K. J.; Spalding, T. R.; Morris, M. A.; Steytler, D. C.; Heenan, R. K.; Schweins, R.; Holmes, J. D. *Langmuir* **2005**, *21*, 4163.

(10) Ghosh, K; Lehmler, H.; Rankin, S. E.; Knutson, B. L. *Langmuir* **2005**, *21*, 6145.

(11) Ghosh, K; Vyas, S. H.; Lehmler, H.; Rankin, S. E.; Knutson, B. L. *J. Phys. Chem. B* **2007**, *111*, 363.

(12) Li, X.; Vogt, B. D. *Chem. Mater.* **2008**, *20*, 3229.

(13) Ghosh, K; Lehmler, H.; Rankin, S. E.; Knutson, B. L. *J. Colloid Interface Sci.* **2012**, *367*, 183.

(14) Cagnol, F; Grosso, D.; Soler-Illia, G. J. A. A.; Crepaldi, E. L.; Babboneau, F.; Amenitsch, H.; Sanchez, C. *J. Mater. Chem.* **2003**, *13*, 61.

(15) Alonso, B.; Balkenende, A. R.; Albouy, P.-A.; Durand, D.; Babboneau, F. *New J. Chem.* **2002**, *26*, 1270.

(16) Yamayauchi, Y.; Sawada, M.; Noma, T.; Ito, H.; Furumi, S.; Sakka, Y.; Kuroda, K. *J. Mater. Chem.* **2005**, *15*, 1137.

(17) Koganti, V. R.; Rankin, S. E. *J. Phys. Chem. B* **2005**, *109*, 3279.

(18) Koganti, V. R. Ph.D. Dissertation, University of Kentucky, 2006.

(19) Ulagappan, N.; Rao, C. N. R. *Chem. Commun.* **1996**, 2759.

(20) Lee, C. T., Jr.; Ryoo, W.; Smith, P. G.; Arellano, J.; Mitchell, D. R.; Lagow, R. J.; Webber, S. E.; Johnston, K. P. *J. Am. Chem. Soc.* **2003**, *125*, 3181.

(21) Callaghan, J. M.; Copley, M. P.; Hanrahan, J. P.; Morris, M. A.; Steytler, D. C.; Heenan, R. K.; Staudt, R.; Holmes, J. D. *Langmuir* **2008**, *24*, 6959.

(22) Johnston, K. P.; Harrison, K. L.; Clarke, M. J.; Howdle, S. M.; Heitz, M. P.; Bright, F. V.; Carlier, C.; Randolph, T. W. *Science* **1996**, *271*, 624−626.

(23) Clarke, M. J.; Harrison, K. L.; Johnston, K. P.; Howdle, S. M. *J. Am. Chem. Soc.* **1997**, *119*, 6399−6406.

(24) Jacobson, G. B.; Lee, C. T. J.; Johnston, K. P. *J. Org. Chem.* **1999**, *64*, 1201.

(25) Holmes, J. D.; Steytler, D. C.; Rees, G. D.; Robinson, B. H. *Langmuir* **1998**, *14*, 6371.

(26) Ji, M.; Chen, X.; Wai, C. M.; Fulton, J. L. *J. Am. Chem. Soc.* **1999**, *121*, 2631.

(27) McLeod, M. C.; McHenry, R. S.; Beckman, E. J.; Roberts, C. B. *J. Phys. Chem. B* **2003**, *107*, 2693.

(28) Yates, M. Z.; Apodaca, D. L.; Campbell, M. L.; Birnbaum, E. R.; McCleskey, T. M. *Chem. Commun.* **2001**, 25.

(29) Ghenciu, E. G.; Russell, A. J.; Beckman, E. J. *Biotechnol. Bioeng.* **1998**, *58*, 572.

(30) Eastoe, J.; Dupont, A.; Steytler, D. C. *Curr. Opin. Colloid Interface Sci.* **2003**, *8*, 267.

(31) Huang, M. H.; Dunn, B. S.; Zink, J. I. *J. Am. Chem. Soc.* **2000**, *122*, 3739.

(32) Minoofar, P. N.; Hernandez, R.; Chia, S.; Dunn, B.; Zink, J. I.; Franville, A.-C. *J. Am. Chem. Soc.* **2002**, *124*, 14388.

(33) Meng, Q.; Fu, L.; Lin, J.; Zhang, H.; Wang, S.; Zhouy, Y.; Yu, M.; Liu, F. *J. Phys. Chem. Solids* **2003**, *64*, 63.

(34) Bartl, M. H.; Scott, B. J.; Wirnsberger, G.; Popitsch, A.; Stucky, G. D. *ChemPhysChem* **2003**, 392.

(35) Gilliland, J. W.; Yokoyama, K.; Yip, W. T. *Chem. Mater.* **2005**, *17*, 6702.

(36) Yao, Y.; Zhang, M.; Shi, J.; Gong, M.; Zhang, H.; Yang, Y. *Mater. Lett.* **2001**, *48*, 44.

(37) Ogawa, M. *Chem. Mater.* **1998**, *10*, 1382.

(38) Hernandez, R.; Franville, A.; Minoofar, P.; Dunn, B.; Zink, J. *J. Am. Chem. Soc.* **2001**, *123*, 1248.

(39) Caragheorgheopol, A.; Caldararu, H.; Vasilescu, M.; Khan, A.; Angelescu, D.; Zÿilkova, N.; Cÿejka, J. *J. Phys. Chem. B* **2004**, *108*, 7735.

(40) Niemeyer, E. D.; Bright, F. V. *J. Phys. Chem. B* **1998**, *102*, 1474.

(41) Liu, D.; Zhang, Z.; Fan, J.; Han, J.; Chen, J. *J. Phys. Chem. B* **2004**, *108*, 2851.

(42) Cao, T.; Johnston, K. P.; Webber, S. E. *Macromoleules* **2004**, *37*, 1897.

(43) Gupta, R. R.; RamachandraRao, V. S.; Watkins, J. J. *Macromoleules* **2003**, *36*, 1295.

(44) Lu, Y.; Ganguli, R.; Drewien, C. A.; Anderson, M. T.; Brinker, C. J.; Gong, W.; Guo, Y.; Soyez, H.; Dunn, B.; Huang, M. H.; Zink, J. I. *Nature* **1997**, *389*, 364.

(45) Yusa, S.; Sakakibara, A.; Yamamoto, T.; Morishima, Y. *Macromolecules* **2002**, *35*, 10182.

(46) Kujawa, P.; Liu, R. C. W.; Winnik, F. M. *J. Phys. Chem. B* **2002**, *106*, 5578.

(47) Kalyanasundaram, K.; Thomas, J. K. *J. Am. Chem. Soc.* **1977**, *99*, 2039.

(48) Ogawa, M.; Igarashi, T.; Kuroda, K. *Chem. Mater.* **1998**, *10*, 1382.

(49) Nakajima, A. *Bull. Chem. Soc. Jpn.* **1971**, *44*, 3272.

(50) Nakajima, A. *Spectrochim. Acta, Part A* **1974**, *30*, 860.

(51) Brennecke, J. F.; Eckert, C. A. *ACS Symp. Ser.* **1989**, *14*, 406.

(52) Brennecke, J. F.; Tomasko, D. L.; Peshkin, J.; Eckert, C. A. *Ind. Eng. Chem. Res.* **1990**, *29*, 1682.

(53) Davis, G. A. *J. Chem. Soc., Chem. Commun.* **1973**, 728.

(54) Wade, D. A.; Tucker, S. A. *Talanta* **2000**, *53*, 571.

(55) Miola, L.; Ab akerli, R. B.; Ginani, M. F.; Filho, P. B.; Toscano, V. G.; Quina, F. H. *J. Phys. Chem.* **1983**, *87*, 4417.

(56) Ayala, J. H.; Afonso, A. M.; Gonzalez, V. *Appl. Spectrosc.* **1997**, *51*, 380.

(57) L'Heureux, G. P.; Fragata, M. *J. Colloid Interface Sci.* **1987**, *117*, 513.

(58) Dominska, M.; Krysinski, P.; Blanchard, G. *Langmuir* **2008**, *24*, 8785.
(59) Chen, S. H.; Frank, C. W. *Langmuir* **1991**, *7*, 1719.
(60) Klaas, Z. A.; Boleslaw, K; Wolfgang, K. *Surfactants Solution, [Proc. Int. Symp.]* **1984**, *1*, 565.
(61) Lissi, E. A.; Gallardo, S.; Sepulveda, P. *J. Colloid Interface Sci.* **1992**, *152*, 104.
(62) Osei-Prempeh, G. Ph.D. Dissertation, University of Kentucky, 2007.
(63) Anandan, C.; Basu, J. B.; Rajam, K. S. *Eur. Polym. J.* **2004**, *40*, 335.
(64) Kukulka-Walkiewicz, J.; Opallo, M. *Solid State Ionics* **2001**, *157*, 263.
(65) Brinker, C. J.; Scherer, G. W. *Sol-Gel Science: The Physics and Chemistry of Sol-Gel Processing*; Academic Press: San Diego, CA, 1989.
(66) Raveendran, P.; Ikishima, Y.; Wallen, S. *Acc. Chem. Res.* **2005**, *38*, 478.
(67) Artaki, I.; Zerda, T.; Jonas, J. *J. Non-Cryst. Solids* **1986**, *81*, 381.
(68) Salazar-Hernandez, C.; Zarraga, R.; Alonso, S.; Sugita, S.; Calixto, S.; Cervantes, J. *J. Sol-Gel Sci. Technol.* **2009**, *49*, 301.
(69) Gibaud, A; Grosso, D.; Smarsly, B.; Baptiste, A.; Bardeau, J.; Babonneau, F.; Doshi, D.; Chen, Z.; Brinker, C.; Sanchez, C. *J. Phys. Chem. B* **2003**, *107*, 6114.
(70) Sabirzyanov, A. N.; Il'in, A. P.; Akhunov, A. R.; Gumerov, F. M. *High Temp.* **2002**, *40*, 231.
(71) The Engineering Toolbox, Retrieved Jun 5, 2010, from: http://www.engineeringtoolbox.com/water-content-compressed-air-d_1275.html.
(72) Tripp, C. P.; Combes, J. R. *Langmuir* **1998**, *14*, 7348.
(73) Hasegawa, M.; Yamasaki, Y.; Sonta, N.; Shindo, Y.; Sugimura, T.; Kitahara, A. *J. Phys. Chem.* **1996**, *100*, 15575.
(74) Kramer, M. C.; Steger, J. R.; Hu, Y.; McCormick, C. L. *Macromolecules* **1996**, *29*, 1992.
(75) Suwa, M.; Hashidzume, A.; Morishima, Y.; Nakato, T.; Tomida, M. *Macromolecules* **2000**, *33*, 7884.
(76) Gonzalez-Garcia, J.; Molina, M. J.; Rodriguez, F.; Mirada, F. *J. Chem. Eng. Data* **2001**, *46*, 918.
(77) Buboltz, J. *Phys. Rev. E* **2007**, *76*, 021903.
(78) Zuniga-Moreno, A.; Galicia-Luna, L. A.; Camacho-Camacho, L. E. *Fluid Phase Equlib.* **2005**, *234*, 151.
(79) Tsekhanskaya, Y. V.; Iomtev, M. B.; Mushkina, E. V. *Russ. J. Phys. Chem.* **1964**, *38*, 1173.
(80) Albo, S.; Muller, E. A. *J. Phys. Chem. B* **2003**, *107*, 1672.
(81) Winnik, F. M. *Polymer* **1990**, *31*, 2125.
(82) McFann, G. J. Ph.D. Dissertation, The University of Texas at Austin, 1993.
(83) McCool, B.; Tripp, C. P. *J. Phys. Chem. B* **2005**, *109*, 8914.
(84) Guney, O.; Akgerman, A. *AIChE J.* **2002**, *48*, 856.
(85) Pathak, P.; Meziani, M. J.; Desai, T.; Sun, Y. *J. Am. Chem. Soc.* **2004**, *126*, 10842.
(86) Liu, H.; Finn, N.; Yates, M. Z. *Langmuir* **2005**, *21*, 379.